folded molecules decreases, there is a corresponding increase in the number of folded molecules (Fig. 2A), and eventually the distribution converges to its equilibrium form at the final concentration of denaturant. The positions of the peaks, however, remain constant, indicating that the average end-to-end distances of the molecules in the subpopulations do not change significantly during the course of the reaction. This is the behavior expected for a two-state system, as inferred for this protein from ensemble methods (*13*, *14*). The fidelity of the technique for measuring accurate kinetics is demonstrated in Fig. 2B, which shows that nearly identical folding rates are obtained from single-molecule data and ensemble stopped-flow measurements.

Whereas the peak positions are constant during the folding reaction, the mean FRET efficiency of unfolded molecules is shifted from 0.51 in the presence of 4 M guanidinium chloride (GdmCl) to 0.64 after mixing is complete and solution conditions are conducive to folding (Fig. 2A). The lower denaturant concentration after dilution results in more compact unfolded molecules, which exhibit higher FRET efficiency. For a Gaussian chain (*16*), this shift would correspond to a decrease in the radius of gyration of about 20% (*9*), which implies a halving of occupied volume. This reconfiguration is obviously complete by the time of the first observation at about 100 ms, consistent with ensemble measurements on other proteins that show collapse of unfolded molecules to be a submillisecond process (*17*–*21*). It is noteworthy that qualitatively different signal changes result from collapse and folding. Collapse of the unfolded state causes a shift of the corresponding peak to higher efficiency, whereas folding increases the folded state population (represented by peak height) and depopulates the unfolded state. This permits separate observations of the two processes. In an ensemble FRET experiment, both collapse and folding would result in an overall increase of the transfer efficiency, and the respective contributions could be identified only indirectly by kinetic modeling.

The power of single-molecule measurements is in the ability to resolve and analyze the properties of subpopulations. The kinetic experiment presented here extends the scope of the technique so that such subpopulations can be studied under conditions far from equilibrium, where they exist only briefly. Experiments in the absence of flow have shown that unfolded Csp must reconfigure quickly relative to the observation time of about 1 ms (*9*), in that no broadening of the measured energy transfer distributions was observed beyond that seen for rigid polyproline peptides. These equilibrium measurements were limited to solution conditions that resulted in sufficiently high concentrations of unfolded molecules. By transiently populating the denatured state with the microfluidic mixer, we can now extend the observations to denaturant concentrations that strongly favor the native structure and are therefore closer to physiologically relevant conditions. The present results (Fig. 3) show that the unfolded peak width is constant to GdmCl concentrations as low as 0.5 M, indicating that, even though there is significant compaction of the unfolded state between 6.0 M and 0.5 M GdmCl, there is no increase in the reconfiguration time beyond the previously calculated limit of 0.2 ms (*22*).

References and Notes

1. T. Ha *et al*., *Proc. Natl. Acad. Sci. U.S.A.* **93**, 6264 (1996).
2. S. Weiss, *Science* **283**, 1676 (1999).
3. X. Zhuang *et al*., *Science* **288**, 2048 (2000).
4. X. Zhuang *et al*., *Science* **296**, 1473 (2002).
5. Y. W. Jia *et al*., *Chem. Phys.* **247**, 69 (1999).
6. E. Rhoades, E. Gussakovsky, G. Haran, *Proc. Natl. Acad. Sci. U.S.A.* **100**, 3197 (2003).
7. A. A. Deniz *et al*., *Proc. Natl. Acad. Sci. U.S.A.* **96**, 3670 (1999).
8. A. A. Deniz *et al*., *Proc. Natl. Acad. Sci. U.S.A.* **97**, 5179 (2000).
9. B. Schuler, E. A. Lipman, W. A. Eaton, *Nature* **419**, 743 (2002).
10. D. S. Talaga *et al*., *Proc. Natl. Acad. Sci. U.S.A.* **97**, 13021 (2000).
11. Materials and methods are available as supporting material on *Science* Online.
12. E. Kauffmann, N. C. Darnton, R. H. Austin, C. Batt, K. Gerwert, *Proc. Natl. Acad. Sci. U.S.A.* **98**, 6646 (2001).
13. D. Perl *et al*., *Nature Struct. Biol.* **5**, 229 (1998).
14. D. Wassenberg, C. Welker, R. Jaenicke, *J. Mol. Biol.* **289**, 187 (1999).
15. The Förster radius R_0 (*11*, *23*) for the dye pair used here is ≈5.4 nm.
16. M. Doi, *Introduction to Polymer Physics* (Oxford, New York, 1996).
17. C. K. Chan *et al*., *Proc. Natl. Acad. Sci. U.S.A.* **94**, 1779 (1997).
18. M. C. R. Shastry, H. Roder, *Nature Struct. Biol.* **5**, 385 (1998).
19. L. Pollack *et al*., *Proc. Natl. Acad. Sci. U.S.A.* **96**, 10115 (1999).
20. S. J. Hagen, W. A. Eaton, *J. Mol. Biol.* **301**, 1019 (2000).
21. S. J. Hagen, C. W. Carswell, E. M. Sjolander, *J. Mol. Biol.* **305**, 1161 (2001).
22. B. Schuler, E. A. Lipman, W. A. Eaton, *Nature* **421**, 94 (2003).
23. B. W. VanDerMeer, G. Coker, S. Y. S. Chen, *Resonance Energy Transfer: Theory and Data* (Wiley, New York, 1994).

24. We thank R. Austin for essential advice and encouragement, K. Schwab for help with microfabrication, and S. Hagen for suggestions regarding the flow system. B.S. was supported by an Emmy Noether fellowship from the Deutsche Forschungsgemeinschaft. O.B.'s work was performed under the auspices of the U.S. Department of Energy under contract no. W-7405-Eng-48 with funding from the Laboratory Directed Research and Development program.

Supporting Online Material

www.sciencemag.org/cgi/content/full/301/5637/1233/DC1
Materials and Methods
Figs. S1 and S2

7 April 2003; accepted 18 July 2003

Single-Molecule Kinetics of λ Exonuclease Reveal Base Dependence and Dynamic Disorder

Antoine M. van Oijen,[1] Paul C. Blainey,[1] Donald J. Crampton,[2] Charles C. Richardson,[2] Tom Ellenberger,[2] X. Sunney Xie[1]*

We used a multiplexed approach based on flow-stretched DNA to monitor the enzymatic digestion of λ-phage DNA by individual bacteriophage λ exonuclease molecules. Statistical analyses of multiple single-molecule trajectories observed simultaneously reveal that the catalytic rate is dependent on the local base content of the substrate DNA. By relating single-molecule kinetics to the free energies of hydrogen bonding and base stacking, we establish that the melting of a base from the DNA is the rate-limiting step in the catalytic cycle. The catalytic rate also exhibits large fluctuations independent of the sequence, which we attribute to conformational changes of the enzyme-DNA complex.

Recent advances in single-molecule enzymatic assays have profoundly changed how biochemical reactions are studied (*1*–*7*). With the removal of ensemble averaging, distributions and fluctuations of molecular properties can be characterized, transient intermediates identified, and catalytic mechanisms elucidated. Here, we report a simple and multiplexed single-molecule assay for studying the mechanisms and dynamics of nucleic acid enzymes.

Individual DNA molecules are attached at one end to a glass surface by a biotin-streptavidin linkage and at the opposite end to polystyrene beads by a digoxigenin-antidigoxigenin linkage (*8*). When a laminar

[1]Department of Chemistry and Chemical Biology, Harvard University, 12 Oxford Street, Cambridge, MA 02138, USA. [2]Department of Biological Chemistry and Pharmacology, Harvard Medical School, 240 Longwood Avenue, Boston, MA 02115, USA.

*To whom correspondence should be addressed. E-mail: xie@chemistry.harvard.edu

flow is applied above the surface (Fig. 1A), the DNA molecules are stretched by a force of 0.1 to 10 pN, proportional to the flow rate and the diameter of the polymer bead. The flow's parabolic velocity profile, with a zero flow rate at the surface, maintains the beads just above the surface. The glass surface is coated with poly(ethylene glycol) to minimize interactions with the beads and enzymes. The lengths of individual DNA molecules can be determined by tracking the positions of the beads with a charge-coupled device camera (1-nm precision of centroid positions). The Brownian motion of the bead in the transverse direction, perpendicular to the flow and parallel to the surface, conveniently serves as a calibration for the stretching force, F. According to the equipartition theorem, the bead's mean-square displacement $\langle \Delta x^2 \rangle$ in this transverse direction is related to F by $\langle \Delta x^2 \rangle = k_B Tl/F$, where k_B is the Boltzmann constant, T is the temperature, and l is the length of the DNA (*9*).

We performed experiments on λ-phage DNA consisting of 48,502 base pairs with a B-form contour length of 16.2 μm. Figure 1B shows the force-extension curves of a single-stranded DNA (ssDNA) and a double-stranded DNA (dsDNA) attached to a 2.0-μm bead measured for the accessible range of flow rates (0 to 15 ml/hour). The data are consistent with previous reports (*10*) and the wormlike chain model (*11*) (Fig. 1B, solid line). The maximum attainable accuracy in the length measurement is determined by the amplitude of the Brownian motion of the bead in the direction along the DNA, characterized by a mean-square displacement of $\langle \Delta z^2 \rangle = k_B T/(\partial F/\partial z)$ (*12*). At a typical force of 2 pN, $\partial F/\partial z$ for both dsDNA and ssDNA (Fig. 1B) gives $\langle \Delta z^2 \rangle^{1/2} \approx 10$ nm. Instabilities in the flow and mechanical drift cause the accuracy to be ~20 nm on the time scale of seconds and ~100 nm on the time scale of hours.

The coiling of ssDNA makes it shorter than dsDNA at low stretching forces (<6 pN). Consequently, a conversion between dsDNA and ssDNA can be monitored by the variation of the DNA length at a constant stretching force (*13*) (Fig. 1B, arrow). The number of nucleotides that are converted can be obtained from the difference in the length between ssDNA and dsDNA. The maximum force accessible with our method is less than that for optical tweezing (*13*) or magnetic trapping techniques (*9*), but the simultaneous wide-field (200 by 200 μm²) observation of many DNA molecules substantially improves the data throughput and statistics.

We used this multiplexed single-molecule method to study the enzymatic activity of λ exonuclease, a 24-kD enzyme required for recombination in bacteriophage λ that degrades each strand of duplex DNA in the 5′ to 3′ direction. The enzyme catalyzes the hydrolysis of phosphodiester bonds in a highly processive manner (*14*). The movement of λ exonuclease along the DNA is driven by the free energy release of hydrolysis and requires no cofactor other than magnesium. The x-ray crystal structure of λ exonuclease revealed a toroidal homotrimer (*14*) that presumably encircles the DNA substrate (Fig. 2A). Because λ exonuclease initiates digestion at a 5′ terminus, our DNA substrate was designed so that only one such terminus is available to the enzyme (*8*), thereby preventing more than one enzyme molecule from acting simultaneously on a particular DNA.

While the sample cell was infused with a buffer containing 500 nM λ exonuclease, a subpopulation of the DNA decreased in length, indicating the enzymatic conversion of dsDNA to ssDNA. We examined about 500 DNA molecules, of which 44 were partially or completely digested. This low fraction is explained by the fact that the

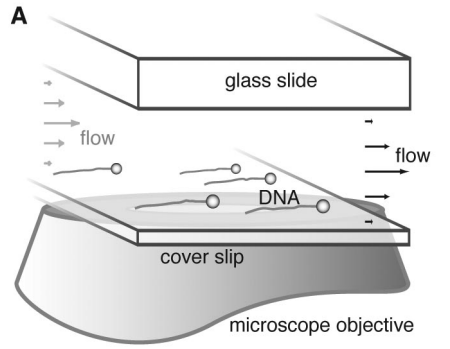

Fig. 1. (**A**) Schematic representation of the experimental arrangement (not drawn to scale). The flow cell is formed by carving a narrow channel out of a 100-μm-thick spacer and sandwiching it between a microscope cover slip and glass slide. (**B**) Extension of λ-phage ssDNA (open circles) and dsDNA (filled circles) as a function of the flow rate, each linked to a 2-μm bead. The right vertical axis displays the corresponding stretching force, based on $F = k_B Tl/\langle \Delta x^2 \rangle$. The gray vertical line at 16.2 μm represents the crystallographic length of B-form λ-phage dsDNA. The dsDNA data are fitted with the wormlike chain model, with a persistence length of 53 nm (*11*). The length shortening of the DNA caused by the enzymatic conversion from dsDNA to ssDNA at the force used in the experiments (2 pN) is illustrated by the horizontal arrow.

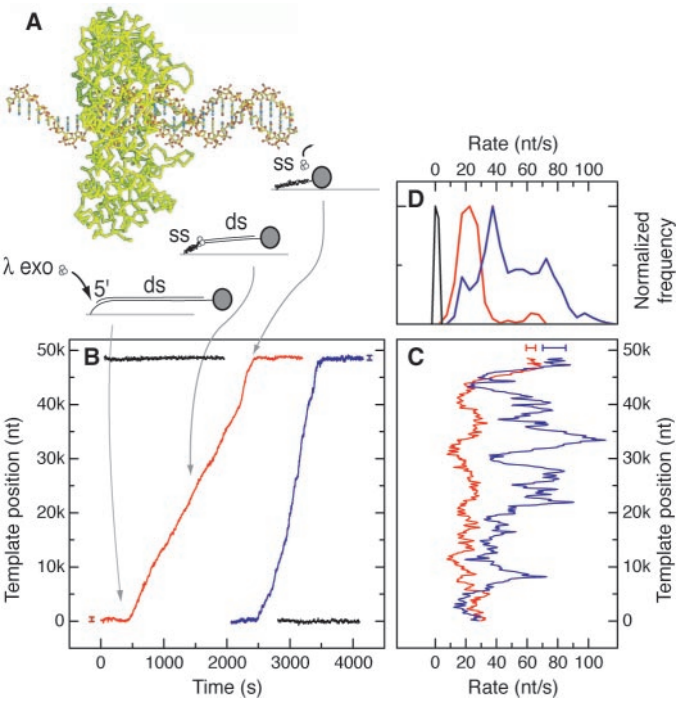

Fig. 2. (**A**) Model of the λ exonuclease–DNA complex, based on crystallographic data [image from (*14*)]. (**B**) Two digestion traces showing complete enzymatic conversion of λ-phage dsDNA into ssDNA. The inaccuracy in reporting the enzyme's position on the template (~400 nt) due to mechanical instabilities is indicated by the error bars. The black traces correspond to simultaneously monitored beads tethered to λ-phage ssDNA (top) and dsDNA (bottom). (**C**) Time derivatives of the two traces from (B) as a function of template position, smoothed over 500 nt. The error bar indicates the error in determining the digestion rate (18 nt/s for the blue trace; 9 nt/s for the red trace). (**D**) Histograms of the digestion rates corresponding to the traces shown in (C). The black curve depicts the experimental uncertainty obtained from the distribution of rates in the ssDNA and dsDNA control traces in (B).

enzyme is a stable trimer that must open to load onto our DNA substrate, which lacks a free 3′ end.

Once the digestion of DNA molecules began, we flushed the chamber with a buffer lacking λ exonuclease. Continued shortening in cases where digestion had started proved that single enzyme molecules are responsible for the processive digestion of DNA. The average processivity of λ exonuclease (the number of base pairs converted to ssDNA before dissociation of the enzyme) during the 44 observed digestion reactions was 18,000 ± 8000 base pairs. The spatial distribution of dissociation events along the λ-phage DNA is discussed in the supporting online material text. The average rate of digestion was 32 nucleotides per second (nt/s) among all digestion trajectories, compared with rates of 18 nt/s (*15*) and ~1000 nt/s (*16*) previously measured with low-resolution single-molecule techniques. Ensemble assays gave a rate of ~12 nt/s (*17*). Underestimation of the digestion rate from ensemble assays is not surprising, because the measurement is complicated by the broadly distributed enzyme processivities, slow binding of the λ exonuclease with the DNA, and uncertainties about the number of enzyme molecules bound to each DNA. These complications are eliminated in single-molecule experiments.

Of the 44 observed digestions, 4 went to completion, with all 48,502 bases of one strand hydrolyzed. Figure 2B shows two of these trajectories, with the digestion rates as a function of template position depicted in Fig. 2C. The digestion rate exhibits large fluctuations during the processive degradation of dsDNA. The distributions of rates during these two full digestions of the DNA are shown in Fig. 2D. DNA molecules that were not being digested were simultaneously monitored as a control to rule out perturbations in the experimental conditions, such as variation in flow rate or mechanical instability, as a cause for the observed fluctuations (Fig. 2B, black traces for both ssDNA and dsDNA). The fluctuations are not reproducible from trace to trace, with a low Pearson's correlation coefficient r of 0.15 ± 0.05 for any two trajectories (*18*). Because r is not distributed symmetrically about zero, a weak correlation must be present. One obvious source of such a correlation is the variation in the DNA sequence encountered by the enzyme.

Despite extensive studies (*14*, *17*, *19*), the catalytic mechanism of λ exonuclease is not well understood. The enzymatic cycle consists of hydrolytic cleavage of a phosphodiester bond in DNA, translocation along the DNA, and melting of the 5′ terminal base from neighboring bases (Fig. 3A). However, the order of these events is not known. Hydrolysis of the phosphodiester bond is thermodynamically favorable, with a free-energy change of –5.3 kcal/mol in the absence of enzyme (*20*), which is expected to be largely independent of the identity of the nucleotides. In contrast, melting of the 5′-terminal base is expected to be sequence-dependent, with the Gibbs free-energy change ΔG°_{melt} having two sequence-dependent contributions. The first is the hydrogen-bonding free energy of a Watson-Crick base pair, which is different for an AT pair (two hydrogen bonds) than for a CG pair (three hydrogen bonds). The second contribution is the free energy of the base-stacking interaction between the 5′-terminal base and its neighboring base in the same strand, which depends on the identity of both bases.

Figure 3B shows the free energies of base stacking (upper trace), hydrogen bonding (center trace), and the sum of the two (lower trace) along the known sequence of λ DNA (GenBank code NC_001416) (*21*, *22*). All curves are smoothed over 500 nt, roughly corresponding to the experimental resolution. The natural variation in the base content of λ-phage DNA gives rise to a distinct modulation of the average thermodynamic properties on experimentally accessible length scales. Even though the presence of enzyme might alter the free energies, it is reasonable to assume that their relative variation along the DNA remains the same.

The sequence dependence of the digestion rate suggests that melting of the base is the rate-limiting step in the catalytic cycle. This notion can be validated by calculating the variation of the digestion rate $\Delta k(n)$ at template position n based on the variation in $\Delta G^\circ_{melt}(n)$ and comparing it with the observed rate. Considering that the variation of the activation barrier is proportional to the variation of $\Delta G^\circ_{melt}(n)$, $\Delta\Delta G^\circ_{melt}(n)$, with a proportionality constant β, the Brønsted value (*23*), the variations in $\Delta k(n)$ are given by $\Delta k(n)/k(n) \approx (-1/k_BT)\beta\Delta\Delta G^\circ_{melt}(n)$ [derived in (*8*)].

Figure 3C shows the average of the rate traces of the four full-length trajectories (black). The data are smoothed over 500 nt, which averages out the stochastic fluctuations of the digestion times for individual bases. The overlaid trace (green, β = 1.2) is the calculated rate fluctuation based on $\Delta G^\circ_{melt}(n)$ (Fig. 3B, lower trace). The ex-

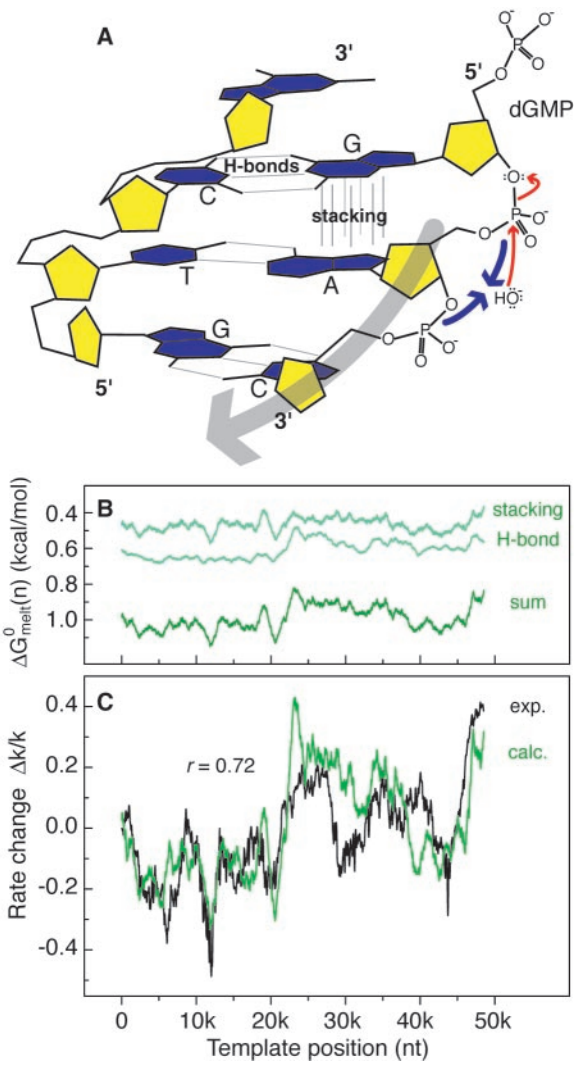

Fig. 3. (**A**) DNA structure pertinent to the products of enzymatic hydrolysis of a phosphodiester bond. Hydrogen-bonding and base-stacking interactions involved in the melting of the terminal guanine are indicated. The gray arrow indicates the 5′ to 3′ direction of enzymatic digestion. The small blue arrows indicate the movement of the scissile and its 3′ neighboring phosphate groups before hydrolysis. Nucleophilic attack of the scissile phosphate by the hydroxide anion is depicted by the red arrows. (**B**) Free energy $\Delta G^\circ_{melt}(n)$ for base melting (bottom trace) along the λ-phage DNA, which is the sum of the hydrogen-bonding (center) and base-stacking components (top). (**C**) Average of experimentally observed rate $\Delta k/k$ along the DNA of four full-length trajectories (black), overlaid with the calculated rate changes (green). All traces in (B) and (C) are smoothed over 500 bases.

perimental and calculated traces are closely correlated with a Pearson's correlation coefficient $r = 0.72$. Lower r values are obtained when either the hydrogen-bonding or the stacking contribution alone is used to calculate $\Delta k(n)$, indicating that both contributions are necessary to account for the observed fluctuations.

The structural similarity of the active-site regions of λ exonuclease and members of the Eco RV family of restriction endonucleases [in particular Eco RV and Pvu II (*24*)] and the common requirement of Mg^{2+} suggest that these proteins share a common catalytic mechanism. Catalysis of this class of restriction endonucleases is substrate-assisted in the sense that an oxygen of the phosphate to the 3′ side of the scissile phosphate deprotonates a water molecule, creating the hydroxide anion that attacks the scissile phosphate (Fig. 3A, red arrows). A motion of the scissile and the 3′ neighboring phosphates toward each other is required for hydroxide generation (Fig. 3A, blue arrows) (*25*). Molecular dynamics simulations on the active site of Pvu II have shown that this decrease in phosphorous-phosphorous distance is accompanied by a large local distortion of the DNA structure (*25*), possibly coinciding with the disruption of Watson-Crick hydrogen bonds and base stacking. Although we could not experimentally resolve whether the rate-limiting base-melting step occurs before or after hydrolysis, these structural considerations allowed us to conclude that it occurs before hydrolysis. The presence of a melting step before hydrolysis has also been implicated for a different exonuclease (*26*). Translocation of the enzyme to the next nucleotide is expected to follow and be driven by the hydrolysis.

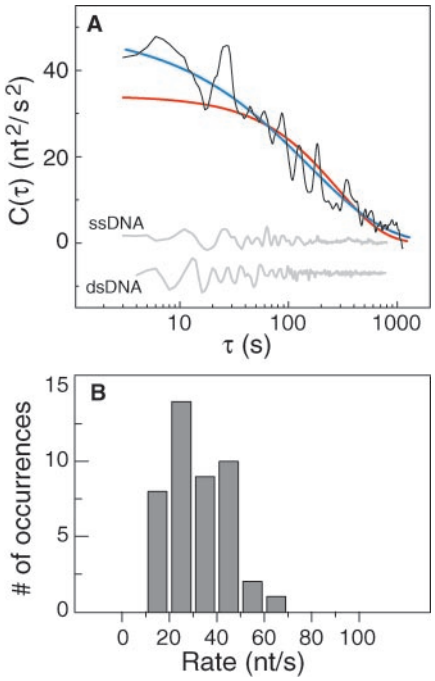

Fig. 4. (**A**) Autocorrelation function of sequence-independent rate fluctuations, calculated from a rate trace of an individual λ exonuclease enzyme digesting λ-phage DNA (black). The red trace represents a single-exponential fit with a decay time of 350 ± 13 s. The blue trace corresponds to a stretched exponential fit $C(\tau) \propto \exp[(\tau/\tau_0)^{\beta}]$, with $\tau_0 = 145 \pm 20$ s and $\beta = 0.5 \pm 0.1$. The autocorrelation functions of traces corresponding to both ssDNA and dsDNA in the absence of digestion are calculated (gray traces), excluding variations in the experimental conditions as a cause for the fluctuations. (**B**) Histogram of the average digestion rates of the first 5000 nt for 44 λ exonuclease molecules.

Each of the four individual rate traces correlates only weakly with the calculated rate trace (average $r = 0.34 \pm 0.1$), indicating that uncorrelated fluctuations mask the sequence-dependent variation. We can distinguish the sequence-independent fluctuations Δk^* in the enzymatic rate from the sequence-dependent modulations by subtracting the averaged rate trace (Fig. 3C, black trace) from the individual single-molecule traces (Fig. 2C). The sequence-independent fluctuations are analyzed by calculating the autocorrelation function of Δk^*, $C(\tau) = \langle \Delta k^*(0) \Delta k^*(\tau) \rangle - \langle \Delta k^* \rangle^2$, where the data are evaluated as a function of time instead of nucleotide position (Fig. 4A, black trace). The time scale of the decay directly indicates the time scale of fluctuations in the enzymatic rate.

A better fit of the measured $C(\tau)$ with a stretched-exponential decay (Fig. 4A, blue trace, normalized $\chi^2 = 0.76$) than with a single-exponential decay (Fig. 4A, red trace, normalized $\chi^2 = 2.29$) suggests the presence of multiple time scales in the rate fluctuations. Previous single-molecule studies have already shown that a single enzyme molecule exhibits dynamic disorder (*4*)—large fluctuations in catalytic rate at a time scale comparable to or longer than the enzymatic cycle—associated with many long-lived conformers undergoing interconversion over a broad range of time scales (*27*, *28*). The existence of dynamic disorder in our system associated with conformational changes of the enzyme-DNA complex is also supported by the broad distribution of digestion rates at the beginning of the 44 digestion traces (Fig. 4B). Static heterogeneity among individual enzyme molecules has been seen previously with time-resolved single-molecule experiments (*29*, *30*). Our time-resolved experiment shows that the initial distribution (Fig. 4B) has a width comparable to the distribution of rates for a single enzyme (Fig. 2D), indicating the existence of slowly interconverting conformers.

The multiplexed nature of our new assay and the natural variation of nucleotide composition in λ DNA allowed us to uncover the sequence dependence of the rate of DNA digestion by λ exonuclease from the more pronounced effect of dynamic disorder. This led to the identification of terminal-base melting as the rate-limiting step in the enzymatic cycle of λ exonuclease and the description of an enzyme as a dynamic entity without a constant catalytic rate, illustrating how single-molecule assays can provide new insights into the catalytic mechanisms of enzymes.

References and Notes

1. J. T. Finer, R. M. Simmons, J. A. Spudich, *Nature* **368**, 113 (1994).
2. T. Funatsu, Y. Harada, M. Tokunaga, K. Saito, T. Yanagida, *Nature* **374**, 555 (1995).
3. H. Yin *et al*., *Science* **270**, 1653 (1995).
4. H. P. Lu, L. Xun, X. S. Xie, *Science* **282**, 1877 (1998).
5. X. Zhuang *et al*., *Science* **288**, 2048 (2000).
6. R. Yasuda, H. Noji, M. Yoshida, K. Kinosita Jr., H. Itoh, *Nature* **410**, 898 (2001).
7. C. Bustamante, Z. Bryant, S. B. Smith, *Nature* **421**, 423 (2003).
8. Materials and methods are available as supporting material on *Science* Online.
9. T. R. Strick, J. F. Allemand, D. Bensimon, V. Croquette, *Biophys. J.* **74**, 2016 (1998).
10. S. B. Smith, L. Finzi, C. Bustamante, *Science* **258**, 1122 (1992).
11. C. Bustamante, J. F. Marko, E. D. Siggia, S. Smith, *Science* **265**, 1599 (1994).
12. T. R. Strick, J. F. Allemand, D. Bensimon, A. Bensimon, V. Croquette, *Science* **271**, 1835 (1996).
13. G. J. L. Wuite, S. B. Smith, M. Young, D. Keller, C. Bustamante, *Nature* **404**, 103 (2000).
14. R. Kovall, B. W. Matthews, *Science* **277**, 1824 (1997).
15. J. Dapprich, *Cytometry* **36**, 163 (1999).
16. S.-I. Matsuura *et al*., *Nucleic Acids Res.* **29**, e79 (2001).
17. K. Subramanian, W. Rutvisuttinunt, W. Scott, R. S. Myers, *Nucleic Acids Res.* **31**, 1585 (2003).
18. Pearson's correlation coefficient r is defined as
$$\frac{n\sum_i^n x_i y_i - \left(\sum_i^n x_i\right)\left(\sum_i^n y_i\right)}{\sqrt{n\sum_i^n x_i^2 - \left(\sum_i^n x_i\right)^2}\sqrt{n\sum_i^n y_i^2 - \left(\sum_i^n y_i\right)^2}}$$
19. P. G. Mitsis, J. G. Kwagh, *Nucleic Acids Res.* **27**, 3057 (1999).
20. K. S. Dickson, C. M. Burns, J. P. Richardson, *J. Biol. Chem.* **275**, 15828 (2000).
21. E. T. Kool, *Annu. Rev. Biophys. Biomol. Struct.* **30**, 1 (2001).
22. S. Bommarito, N. Peyret, J. SantaLucia Jr., *Nucleic Acids Res.* **28**, 1929 (2000).
23. A. Fersht, *Structure and Mechanism in Protein Science* (Freeman, New York, 1999).
24. R. A. Kovall, B. W. Matthews, *Proc. Natl. Acad. Sci. U.S.A.* **95**, 7893 (1998).
25. C. Rauch *et al*., *J. Mol. Biol.* **324**, 491 (2002).
26. W.-C. Lam *et al*., *Biochemistry* **41**, 3943 (2002).
27. H. Frauenfelder, S. G. Sligar, P. G. Wolynes, *Science* **254**, 1598 (1991).
28. X. S. Xie, *J. Chem. Phys.* **117**, 11024 (2002).
29. Q. Xue, E. S. Yeung, *Nature* **373**, 681 (1995).
30. R. Polakowski, D. B. Craig, A. Skelley, N. J. Dovichi, *J. Am. Chem. Soc.* **122**, 4853 (2000).

31. We thank A. Goel and D. Herschbach for helpful discussions. This work is funded by NIH (grant 5R01GM61577-03 to X.S.X. and #R01GM55390-07 to T.E.). A.M.v.O. thanks the Human Frontier Science Program for financial support.

Supporting Online Material

www.sciencemag.org/cgi/content/full/301/5637/1235/DC1
Materials and Methods
SOM Text
Figs. S1 to S4
References
Movie S1

11 March 2003; accepted 18 July 2003